The definitive publisher version is available online at https://doi.org/10.1016/j.jwpe.2022.103185

Magnetic spent coffee biochar (Fe-BC) activated peroxymonosulfate system for humic acid removal from water and membrane fouling mitigation

Yatong Li[a,b], Xinbo Zhang[a,b,*], Huu Hao Ngo[c,a*], Wenshan Guo[c,a], Dan Zhang[a,b], Huizhong Wang[a,b], Tianwei Long[a,b]

[a]*Joint Research Centre for Protective Infrastructure Technology and Environmental Green Bioprocess, School of Environmental and Municipal Engineering, Tianjin Chengjian University, Tianjin 300384, China*
[b]*Tianjin Key Laboratory of Aquatic Science and Technology, Tianjin Chengjian University, Jinjing Road 26, Tianjin 300384, China*
[c]*Centre for Technology in Water and Wastewater, School of Civil and Environmental Engineering, University of Technology Sydney, Sydney, NSW 2007, Australia*

*Correspondence authors: Email: zxbcj2006@126.com (X. B. Zhang);

ngohuuhao121@gmail.com (H. H. Ngo)

Abstract

Applying membrane technology to water purification has been done for several decades now and is widespread. However, membrane fouling is a serious problem and continues to limit the success of membrane processes. In this study, magnetic biochar (Fe-BC) was prepared using easily available spent coffee grounds to activate peroxymonosulfate (PMS) as a UF membrane pretreatment strategy. Results showed that the average removal rates of humic acid (HA, 10 mg/L) were 55.23% and 73.55%, at the Fe-BC dosage of 300 mg/L and PMS dosage of 300 mg/L and 900 mg/L, respectively. The Fe-BC/PMS pretreatment significantly reduced the total (44%) and reversible (61%) UF membrane fouling after five filtration cycles at a relatively high flux of 200 L/m^2·h, and the Fe-BC and PMS dosage of 100 mg/L. Modeling fit results indicated that pretreatment shifted complete blocking to standard blocking. Therefore, stopping HA-induced membrane fouling could be possible if the load is reduced and complete blocking alleviated.

Keywords: Magnetic biochar; Peroxymonosulfate; Humic acid; Membrane fouling.

1. Introduction

The ultrafiltration (UF) process is recognized as a safe drinking water treatment technology because of its excellent retention performance, simple operation and low working pressure. It has been gradually applied at home and abroad in the past few decades [1,2]. Due to the complex composition such as chemicals and substances within surface water, serious membrane fouling caused by natural organic matter (NOM) during actual operation has become a major issue, limiting the widespread application of UF membranes [3,4]. Humic acid (HA), commonly present in surface water, has become the main organic material causing membrane fouling in the water treatment process [5,6]. As well, the large amount of HA not only affects the chromaticity of water, increases the solubility of micro-pollutants in water, but also compounds with micronutrients in water or forms complexes with residual pesticides and metal ions. Consequently, it raises the difficulty of water treatment and accelerates the rate of UF membrane fouling [7,8]. For these reasons, removing HA from water is necessary for producing high water quality and stopping membrane fouling.

In recent years, researchers have conducted numerous studies (e.g., low flux operation, pretreatment, membrane modification, chemical cleaning, intermittent pumping) in order to alleviate UF membrane fouling caused by NOM in the membrane

water treatment process, and improve the quality of residential water [9]. The membrane pretreatment process is of great concern. The pretreatment process can change the physical, chemical and biological characteristics of surface water, enhance the removal of some pollutants in water, reduce the membrane treatment load, and alleviate membrane pollution [10]. The relatively mature pretreatment processes include coagulation [11], adsorption [12], ion exchange [13], and oxidation pretreatment [14,15]. However, conventional pretreatment processes have certain limitations, such as coagulation and adsorption pretreatment can easily cause secondary pollution, and do not prevent irreversible pollution [16]. Ion exchange pretreatment does not mitigate membrane fouling very well and the pH range in applications is small [17,18]. Oxidation pretreatment creates unfavorable intermediate by-products and poor efficiency [19].

In addition, advanced oxidation processes (AOPs) were proposed as pretreatment coupling with membrane filtration technology for water purification. AOPs can directly mineralize certain organic pollutants in water by *in situ* generation of highly reactive oxygen species such as hydroxyl (·OH) or sulfate ($SO_4^{\cdot-}$) radicals, and have been rapidly devised for practical applications. AOPs are based on the generation of ·OH or superoxide radicals ($O_2^{\cdot-}$) Fenton, Fenton-like oxidation [20], ozone oxidation [21], ultrasonic oxidation [22], and photocatalytic oxidation [23,24]. Of these, the sulfate radical-advanced oxidation processes (SR-AOPs) based on producing $SO_4^{\cdot-}$ has been widely used in water treatment and groundwater remediation. Compared with ·OH (1.80~2.70 V; $t_{1/2}$<1 μs), $SO_4^{\cdot-}$ (2.60~3.10 V; $t_{1/2}$= 30~40 μs) has the advantages of high standard redox potential, long half-life, high selectivity for pollutants, fast reaction rate, and wide pH applicability. Furthermore peroxymonosulfate (PMS) retains higher stability and is less expensive than H_2O_2 [25]. So using SR-AOPs as pretreatment for UF is an ideal way to remove organic pollutants and mitigate membrane fouling. PMS itself is relatively stable in nature and does not easily generate radicals spontaneously. Nevertheless, they can be generated by external energy (UV, ultrasound, microwave, heat, etc.), carbonaceous materials, transition metals and their oxides activation [26]. Biochar has the advantages of being economical and easy availability of raw materials, high specific surface area, rich oxygen-containing functional groups and stable properties. Using biochar as a catalyst for PMS can remove HA and slow down membrane fouling by the dual action of oxidation and adsorption [27]. Furthermore, magnetic biochar not only improves the reusability and recyclability of biochar, but also accelerates the activation rate of PMS by incorporating iron [28]. In this way, magnetic biochar activating PMS as pretreatment

coupling with UF membrane technology can effectively alleviate membrane fouling and guarantee the effluent quality.

In this work, magnetic biochar (Fe-BC) was prepared by the co-precipitation method using spent coffee grounds for activating PMS before UF. The effectiveness of Fe-BC /PMS pretreatment was evaluated in mitigating UF membrane fouling caused by HA. The objectives were to: (1) prepare and characterize the magnetic biochar derived from spent coffee grounds; (2) investigate the HA removal performance of Fe-BC/PMS pretreatment; (3) evaluate the performance of catalytic systems in mitigating membrane fouling; and (4) explore the mechanism of membrane fouling mitigation.

2. Materials and methods

2.1. Reagents and materials

Spent coffee grounds were collected from a cafe in Tianjin, China. Humic acid (HA) was purchased from Aladdin, China. Potassium peroxomonosulfate ($2KHSO_5 \cdot KHSO_4 \cdot K_2SO_4$ PMS, 99%) was obtained from Shanghai Macklin Biochemical Share Co., Ltd. (Shanghai, China). Sulfuric acid (H_2SO_4), sodium hydroxide (NaOH), tert-butanol (TBA), methanol (MeOH) and ethanol absolute were sourced from Tianjin Jindongtianzheng Precision Chemical Reagent Factory (Tianjin, China). Ferrous sulfate heptahydrate ($FeSO_4 \cdot 7H_2O$) and Ferric trichloride hexahydrate ($FeCl_3 \cdot 6H_2O$) were bought from Tianjin Damao Chemical Reagent Factory (Tianjin, China). All reagents or chemicals were of analytical grade. Polyvinylidene fluoride ultrafiltration membrane (PVDF) was obtained from a company in Beijing and the substance had a molecular weight cut-off (MWCO) of 100 KDa, pure water permeance of 142.80 L/($m^2 \cdot h \cdot bar$) and water contact angle of 68.59° (see Fig. S1). In effect it was a hydrophilic membrane.

2.2. Experimental procedures

2.2.1. Preparation of magnetic coffee grounds biochar

The magnetic biochar was prepared by co-precipitation with some modifications [29]. Key steps were given as follows (see Fig. 1). First, the dried coffee grounds were sieved through a 100 mesh screen. Next 5.00 g of sieved coffee grounds were added to 250 ml of mixed iron salts (8.34 g $FeSO_4 \cdot 7H_2O$ and 16.21 g $FeCl_3 \cdot 6H_2O$) and stirred magnetically for 30 min. Then pH was adjusted to 10~11 with 5 M NaOH and continually

stirred for 30 min. The mixture was left for 18 h. During this time, the reaction in Eq. (1) occurred. The pH of the supernatant was neutral after washing. Afterwards the sediments were dried at 65 °C. Under limited oxygen conditions, the dried sediments were pyrolyzed in a muffle furnace at 600 °C (5 °C/min) for 2 h. After cooling, they were washed again and dried to constant weight at 105 °C. Finally, the magnetic biochar was obtained and named Fe-BC. The same operation described above was done without adding iron salts, and the biochar obtained was named BC.

$$Fe^{2+} + Fe^{3+} + 8OH^- \rightarrow Fe_3O_4 + 4H_2O \quad (1)$$

2.2.2. Experimental set up

To explore the effect of the catalytic oxidation system on HA removal under different conditions, batch experiments were conducted in conical flasks. The dosage of catalyst and oxidant dosing (10, 30, 50, 100, 200, 300, 400, 500 mg/L) was optimized in priority under the following operations. First, a 10 mg/L HA simulant was prepared by mixing the HA stock solution with deionized water and the pH adjusted to 6 (0.1 M H_2SO_4 or NaOH). Next BC or Fe-BC and PMS were added sequentially to a conical flask containing 100 ml of HA simulant. The reaction was shaken in a constant temperature shaker (25 ℃, 200 rpm) for 2 h and stopped immediately after adding 1ml of methanol. Then the HA solution was filtered through a 0.45 μm filter membrane. Finally, the HA concentration was measured by UV spectrophotometer at 254 nm. The following beaker experiments were subsequently performed by changing the corresponding conditions.

The effects of initial pH (5, 6, 7, 8 and 9), reaction time (within 8 h) and coexisting ions (Cl^-, HCO_3^-, CO_3^{2-}, NO_3^- and $H_2PO_4^-$) on the reaction system were investigated. The contribution of ·OH and $SO_4^{\cdot-}$ to the degradation of HA was investigated utilizing quenching experiments. MeOH (scavenging $SO_4^{\cdot-}$ and ·OH) and TBA (scavenging ·OH) served as quenching agents with a molar ratio of quencher to oxidant of 1500 [30]. Meanwhile, newly prepared Fe-BC was kept in a sealed storage for 20, 40 and 70 days and then used to test its stability. Reused and regenerated catalysts tested its reusability and regeneration. Here the reused catalyst was obtained from used Fe-BC after ultrasonic (5 min), washing and drying. The regenerated catalyst was obtained by re-pyrolysis in a muffle furnace.

The schematic of the ultrafiltration experimental set up is illustrated in Fig. 1. The process was run with dead-end filtration and a peristaltic pump maintained a constant flux (200 L/(m^2·h)). Before the experiment, UF membranes were pre-soaked with ultrapure

water for 2 h and filtered for 10~15 min to keep the trans-membrane pressure (TMP) stable. The TMP was recorded automatically using a pressure recorder. The effective filtration diameter of membrane cell was 3.1 cm. Single cycle filtration time was 2 h, multi-cycle filtration experiment included five filtration cycles and each cycle consisted of filtration for 1 h and backwash for 3 min with a double flux. To investigate the effect of HA removal rate on membrane fouling during Fe-BC/PMS pretreatment, single-cycle filtration experiments were conducted after 2 min, 0.5 h, 1 h, 2 h and 8 h of reaction, respectively.

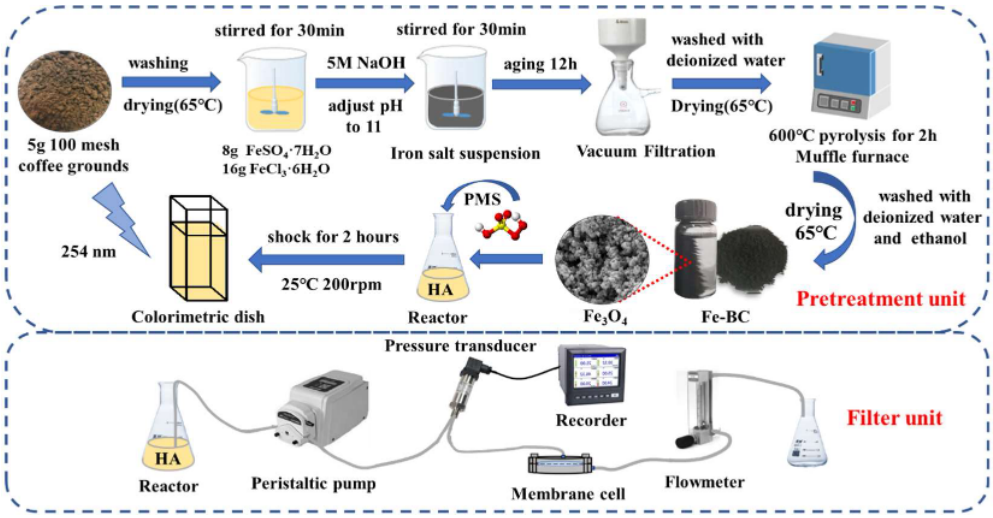

Fig. 1. Schematic diagram of the experimental procedure.

2.3. Fouling resistance analysis

The structure and distribution of membrane fouling were quantified by the resistance-in-series model, while individual fouling component was calculated from the TMP using Darcy's Law [31], as shown in Eq. (2)~(4):

$$R_t = TMP/\mu J \quad (2)$$

$$R_t = R_m + R_r + R_{ir} \quad (3)$$

$$R_f = R_r + R_{ir} \quad (4)$$

Where: TMP is the trans-membrane pressure (Pa); J denotes the permeate flux (L/m^2·h); μ is the dynamic viscosity of the water samples (Pa·s); Rt (m^{-1}) stands for the total hydraulic resistance. Rm, Rr, and Rir are the intrinsic membrane resistance (m^{-1}), hydraulic reversible resistance (m^{-1}) and irreversible resistance (m^{-1}), respectively. In this

study, Rm was determined by the filtration test of ultrapure water and the trans-membrane pressure was recorded as TMP_0, and calculated as Eq. (5). After filtering the water sample for 1 h, the trans-membrane pressure was recorded as TMP_1. Following double flux backwashing, the trans-membrane pressure in forward filtration of ultrapure water was recorded as TMP_2. Then Rr and Rir can be calculated by Eqs. (6) and (7):

$$R_m = TMP_0 / \mu J \quad (5)$$

$$R_r = \left(TMP_1 - TMP_2\right) / \mu J \quad (6)$$

$$R_{ir} = \left(TMP_1 - TMP_2 - TMP_0\right) / \mu J \quad (7)$$

$$P' = 1 + FI \times V_{SP},\ P' = TMP / TMP_0 \quad (8)$$

Added to this, the membrane fouling index (FI, m^{-1}) could be calculated from Eq. (8) to document the extent of membrane fouling [32,33]. Here, P' is the normalized trans-membrane pressure and Vsp (m^3/m^2) is the filtration volume per unit membrane area.

2.4. Fouling models analysis

In the actual ultrafiltration process, membrane fouling may be caused by several fouling behaviors simultaneously. It is difficult to explain the mechanism of membrane fouling with typical membrane fouling models [19]. Hence, five combined fouling models (Table S1) were introduced including cake-complete, cake-intermediate, complete-standard, intermediate-standard, cake-standard blocking models [34]. In this study, the curve changes in the TMP were fitted by the combined models, and the degree of model fit was evaluated based on the correlation coefficient R^2.

2.5. Analysis Methods

The morphology of catalysts was analyzed by Scanning electron microscope (SEM, Hitachi Regulus 8100, Japan). The elemental composition of biochar before and after modification was measured by X-ray photoelectron spectrometry (XPS, K-alpha, USA). The chemical composition and surface functional groups of biochar before and after modification were determined using Fourier transform infrared spectroscopy (FTIR, Is10, USA). The concentration of HA was analyzed by UV–Vis spectrophotometer (Shimadzu, UV-2600) at 254 nm, while the contact angle of UF membrane surface was measured by water contact angle tester (CA, JC2000DF, China). The DOC was analyzed by a total

organic carbon analyzer (TOC-VWP, Japan).

The HA removal efficiency (R_{HA},%) was calculated using Eq. (9), where C_0 is the initial HA concentration and Ct is the post-reaction concentration. Specific ultraviolet absorbance (SUVA, L/mg·cm) was employed to indirectly respond to the change in hydrophobicity of the HA solution before and after pretreatment [35]. Calculated as in Eq. (10), where λ is the absorbance (cm^{-1}) and DOC is dissolved organic carbon (mg/L):

$$R_{HA} = \left(C_0 - C_t\right)/C_0 \times 100\% \quad (9)$$

$$SUVA = \lambda / DOC \times 100 \quad (10)$$

3. Results and Discussion

3.1. Characterizations of the catalysts

The surface morphology of BC and Fe-BC were analyzed by SEM. As depicted in Fig. 2a~c, the particle size of BC varied and had a broken, irregular structure in appearance, which was due to the aromatization and carbonization of cellulose and other tissues during the pyrolysis of coffee grounds. In addition, the surface exhibited obvious irregular pores, which was caused by the collapse of the pores' structure at relatively high temperatures [36]. It could be seen from Fig. 2d~f that a large number of microspheres were loaded onto the Fe-BC surface forming a rough surface, which resulted from the morphological transformation of iron ions during the co-precipitation process. In addition, compared with BC, the particle size of Fe-BC was more heterogeneous, while the surface was smoother and more regular. On one hand, this was due to the acidic environment caused by iron salt hydrolysis. It led to acidification corrosion of the cellulose and other structures in coffee grounds. On the other hand, it was because the formed magnetic microspheres were closely loaded on the surface of biochar and covered the original pores. According to the SEM analysis, iron was successfully loaded on the surface of biochar by the co-precipitation method.

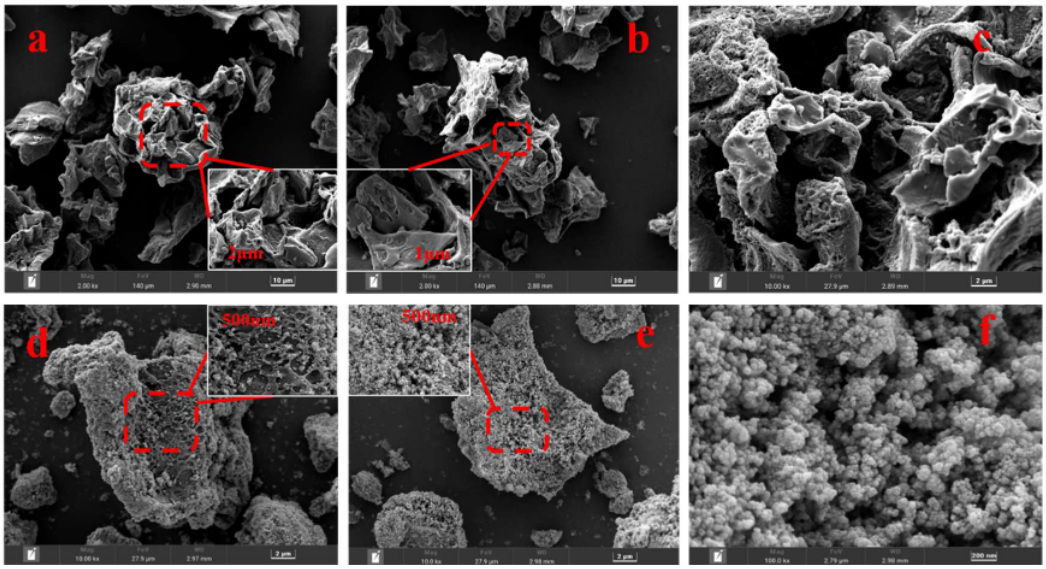

Fig. 2. SEM images of BC (a-c) and Fe-BC (d-f).

The FTIR spectra of BC and Fe-BC (see Fig. S2) showed similar positions and intensities of the characteristic peaks. For example, a broad peak existed at a wavenumber of 3430 cm^{-1}, which was caused by O-H bond tensile vibrations in the hydroxyl or interlayer crystal water [37]. The peak at 1080 cm^{-1} was due to the tensile vibrations of the C-O-H bond in the carboxyl group and phenol. The peaks near 2922 cm^{-1}, 1384 cm^{-1} and 879 cm^{-1} were attributed, respectively, to the tensile vibrations of C-H bonds in aliphatic functional groups and alkyl, lignin, carbohydrates, and aromatic groups. The peak near 1629 cm^{-1} resulted from C=O and C=C bond tensile vibrations in the carbonyl or aromatic group [26]. Compared to BC, the spectra of Fe-BC exhibited a clear characteristic peak formed by Fe-O bonding near 570 cm^{-1}, which confirmed the formation of iron oxides and the successful loading on biochar [38]. Apart from this, the intensity of the C-O-H characteristic peak of Fe-BC waned and C=C was enhanced due to the formation of a Fe-O bond [6]. The above results demonstrated that the surface of BC and Fe-BC was rich in oxygen-containing functional groups such as -OH, -C=O- and -COOH, which would be important active sites for activation of persulfate [39]. It could also be inferred that the oxygen-containing functional groups on the biochar surface are involved in the activation of PMS.

The full-spectrum and single element spectra (Fe2p, C1s and O1s) of Fe-BC and BC were analyzed by XPS, and the results are depicted in Fig. S3. The elemental contents of C, O, N, and Fe in BC were 66.79%, 6.98%, 18.48%, and 0.18%, respectively. The corresponding elemental contents in Fe-BC were 34.61%, 37.73%, 8.33%, and 19.33%, respectively. Compared to BC, Fe-BC had a lower C/O ratio and a higher Fe content. This

was because Fe replaced some of the C and combined with oxygen elements to form Fe-O bonds during the modification process [38]. This was consistent with the conclusions drawn from the analysis of FTIR (see Fig. S2). In Fig. S3d, as seen in the Fe2p spectra of Fe-BC, the peaks at binding energies of 709.08 eV and 723.64 eV were caused by Fe $2p_{3/2}$, the peaks at 711.90 eV, 713.41 eV and 726.35eV resulted from Fe $2p_{1/2}$. The peaks at 718.20 eV and 732.48 eV were the satellite peaks of Fe $2p_{3/2}$ and Fe $2p_{1/2}$, respectively [40]. In general, Fe(III) and Fe(II) correspond to the peak produced by Fe $2p_{1/2}$ and Fe $2p_{3/2}$, respectively. Therefore, the peak area ratio of Fe(II) to Fe(III) could be obtained from the Fe2p spectrum as approximately 1: 2. It meant that the presence of Fe in Fe-BC was mainly Fe_3O_4. Fig. S3b and c also present the generation of Fe-O bonds and the existence of abundant oxygen-containing functional groups, which revealed the potential of Fe-BC to activate PMS.

3.2. Performance of catalytic oxidation systems

3.2.1. Effect of Fe-BC and PMS dosage on HA removal

The appropriate dosage of activator and catalyst are key factors in the actual persulfate-coupled UF process. Therefore, the effects of Fe-BC and PMS dosage on HA removal were investigated. As shown in Fig. 3a, when the PMS dosage was 100 mg/L, the HA removal rate rose gradually with the increase of Fe-BC dosage (10~500 mg/L). The removal rate of HA can reach up to 56.34% at the Fe-BC dosage of 500 mg/L. This was due to the addition of Fe-BC providing more active sites and iron oxide, hence they facilitated the activation of PMS to generate more radicals for the degradation of HA [41]. The increase of Fe-BC provided wider adsorption area and facilitated the physical removal of HA. The effect of PMS dosage on HA removal under the scenario of Fe-BC dosage of 100 mg/L is shown in Fig. 3b. With the increase of PMS dosage (10~500 mg/L), the removal rate of HA by the system showed an upward trend first and then diminished. When the dosage of PMS was 300 mg/L, the removal rate of HA was highest (40.38%). This was because higher oxidant dosage generated more radicals, which contributed to the degradation of organic matter. However, excess PMS generated a large amount of $SO_4^{\cdot-}$ in a short period of time and occurred in radical quenching reaction (see Eq. (11)) [42], which reduced the radical concentration and degradation efficiency. From Fig. 3, it could be seen that the best concentration ratio of Fe-BC to PMS was 1: 3. However, considering the problems such as secondary pollution caused by sulfate in actual

operation, the concentration ratio of Fe-BC to PMS was chosen as 1: 1 in this study:

$$2SO_4^{\cdot-} + HSO_5^- \rightarrow 2SO_4^{2-} + HSO_5^{\cdot-} \quad (11)$$

Additionally, in order to investigate the maximum removal capacity of the Fe-BC/PMS system for HA, the experiments were conducted at concentration ratios of 1: 1 and 1: 3, respectively. As shown in Fig. S4, the removal rates of HA in both systems tended to increase when the catalyst and oxidant dosage increased. The removal rate of HA was 60.76% when both Fe-BC and PMS were dosed at 400 mg/L. It reached up to 73.55% as Fe-BC and PMS were dosed at 300 mg/L and 900 mg/L, respectively. This showed that the system had a strong HA removal capacity. As UF pretreatment, the Fe-BC and PMS dosage were both selected to be 100 mg/L, in view of the cost of the agent and the rate of HA removal increase. If not specified, this concentration was applied in all subsequent experiments. At the same time, four systems of PMS alone, Fe_3O_4/PMS, BC/PMS, and Fe-BC/PMS were conducted to verify the superiority of coupling biochar and iron salts in activating PMS for removing HA (see Fig. S5). The results showed that the Fe-BC/PMS system functioned well in HA removal under both dosing conditions, confirming the superior performance of magnetic biochar in activating PMS.

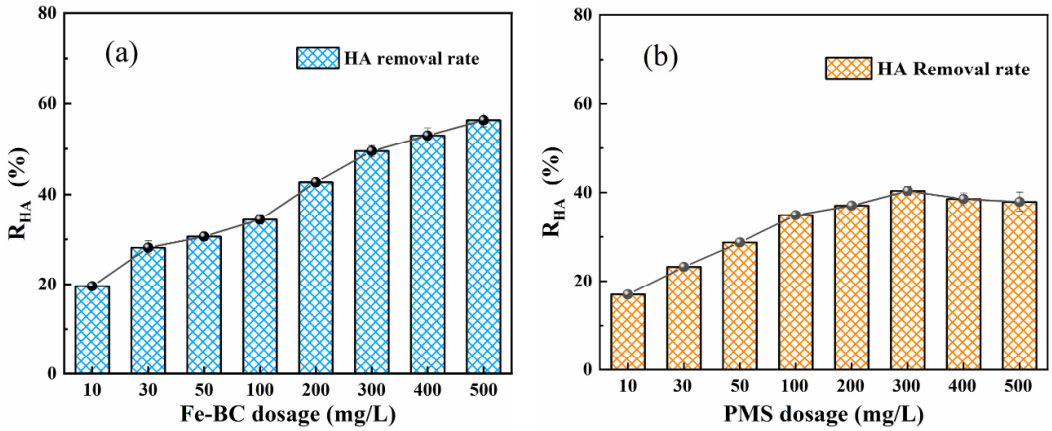

Fig. 3. Effect of Fe-BC dosage (a) and PMS dosage (b) on HA removal.

3.2.2. Effect of reaction conditions on HA removal

The initial pH of the solution usually affects the degradation system by influencing the surface characteristics of the catalyst, the oxidant stability, the morphology of the compound and the radical species [29,43]. In this study, the effect of Fe-BC/PMS system on HA removal under different initial pH (5~9) conditions was investigated. As shown in Fig. 4a, the initial pH had no significant effect on HA removal. This was due to the fact that weak acids such as carbonic acid were produced by PMS during the degradation

reaction [44], resulting in lower pH and gradual stabilization in the systems, and subsequently the systems eventually achieved similar degradation effects. The above outcomes indicated that the pretreatment system can be applied in a wide range of pH, and had great potential in actual water treatment. The ability of the Fe-BC/PMS system to degrade organic matter would be greatly reduced under strong acid or strong alkali conditions. On one hand, because the corrosion of iron oxide would be accelerated under extremely acidic conditions, and Fe^{2+} combined with water to become hydrate or coupled with proton to form Fe^{3+} (Eq. (12)~(14)), as a result losing the ability to activate PMS [45]. On the other hand, due to the hydrolysis of iron salts in the strong alkali conditions, the catalyst surface can be attached by a layer of iron oxides or hydroxyl oxide complexes. This prevented further corrosion of Fe-BC, and thus limited the degradation of organic matter [46]:

$$Fe^{2+} + 5H_2O \rightarrow \left[Fe\left(6H_2O\right)_5\right]^{2+} \quad (12)$$

$$Fe^{2+} + 6H_2O \rightarrow \left[Fe\left(6H_2O\right)_6\right]^{2+} \quad (13)$$

$$Fe^{2+} + 6H_2O + H^+ \rightarrow \left[Fe\left(6H_2O\right)_6\right]^{3+} \quad (14)$$

The efficiency in degrading organic matter is another important indicator whether AOPs can be used in practice. Thus the effect of reaction time on the HA removal by Fe-BC/PMS system was investigated, and the result is shown in Fig. 4b. Under different catalyst and oxidant dosages conditions, the removal of HA in three reaction systems occurred mainly in the first 1 h, and could reach more than 50% of the total removal rate within 15 min. As the reaction proceeded, the concentration of HA gradually stabilized. The removal rates of HA for the three systems were 40%, 60%, and 78% at the end of 8 h, respectively. This indicated that the Fe-BC/PMS system presented the characteristics of rapid reaction and high efficiencies in generating radicals to degrade organic matter.

In the advanced oxidation process, the anions in surface water can affect the removal efficiency of organic matter to different degrees by combining with radicals [47]. In order to better apply the Fe-BC/PMS pretreatment system to practical engineering, the effects of Cl^-, HCO_3^-, CO_3^{2-}, NO_3^- and $H_2PO_4^-$ as interfering ions were investigated. As can be seen from Fig. 4c, five ions all displayed the same trend in the influences on the reaction system at concentrations of 5 mM and 10 mM, respectively. It had been reported that Cl^- could react with $SO_4^{\cdot-}$ and ·OH through a series of reversible chain reactions (see Table S2) to form low oxidation activity chlorine-containing radicals in the AOPs, which inhibited the degradation of organic pollutants [48]. However, in the lower Cl^-

concentration range the opposite result appeared [49], which was consistent with this study. This was because Cl^- increased the ionic strength in the reaction system, which would facilitate the electron transfer between Fe-BC surface and PMS to generate more radicals, thus improving the degradation efficiency of organic matter [50].

Different from the catalytic system containing Cl^-, the results showed that HCO_3^-, CO_3^{2-}, NO_3^- and $H_2PO_4^-$ inhibited HA degradation to varying degrees. In fact, HCO_3^- and CO_3^{2-} had the most inhibitory effect because they generated species with low or no oxidation capacity due to irreversible reaction with radicals (see Table S2) [51]. In addition, HCO_3^- and $H_2PO_4^-$ as buffer ions can increase the pH of the Fe-BC/PMS reaction system. This led to inhibiting the production of iron ions on the surface of biochar or reduction of the oxidation potential of radical species [52]. Moreover, $H_2PO_4^-$ complexed with iron species or occupied the active center of the catalyst [53]. All mentioned above behaviors had adverse effects on HA degradation.

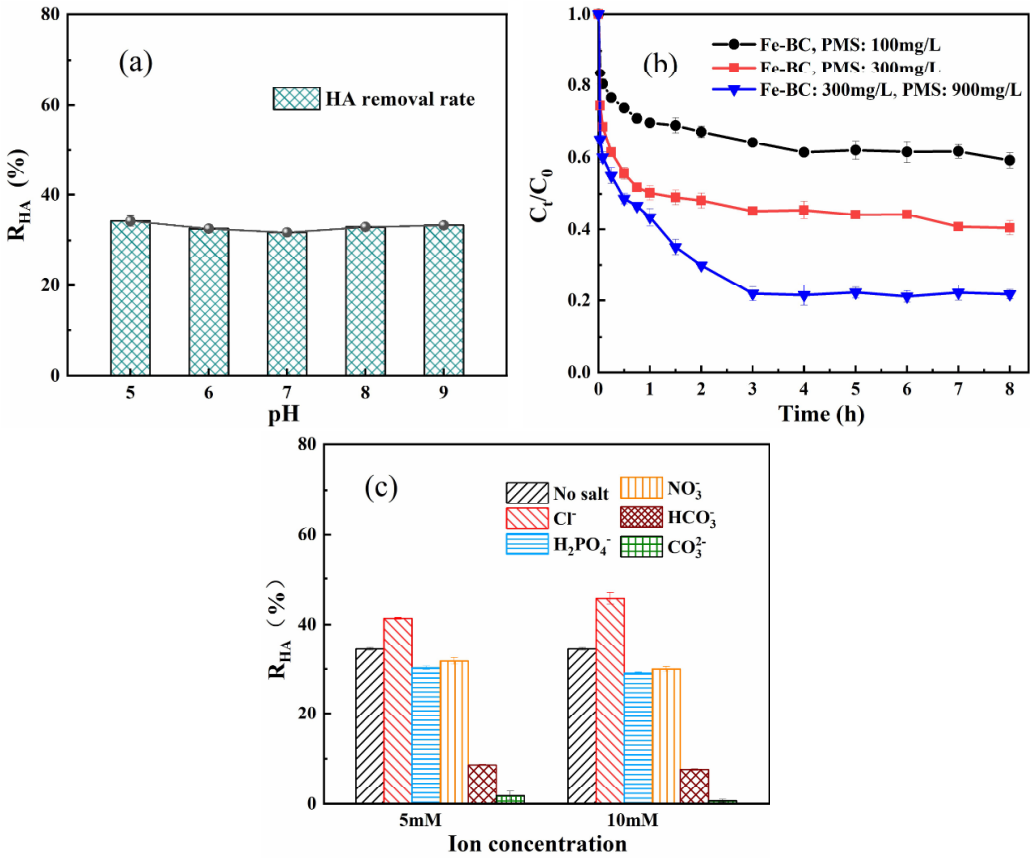

Fig. 4. Effect of initial pH (a), reaction time (b), and coexisting ions (c) on HA removal.

3.2.3. HA removal mechanism

In the Fe-BC/PMS system, the removal of HA is the result of a combination of modalities. One of the ways was the degradation by active species such as ·OH and $SO_4^{\cdot-}$

[54]. On one hand, the radicals were generated owing to the activation of PMS by persistent free radicals, defective sites and oxygen-containing functional groups in the biochar. On the other hand, they were mainly produced by heterogeneous activation of PMS by the loaded magnetic iron oxide via the reactions in Eqs. (15) and (16). To identify the possible reactive species in the system, quenching experiments were conducted in Fig. 5. With only PMS, the removals of HA were 15.70% and 20.62% under the two experimental conditions, respectively, which meant that it could degrade HA directly through the nonradical pathway. So this became a dominant mode when the dosage was small. After the addition of TBA, the HA removal rate in two Fe-BC/PMS systems was significantly inhibited, which declined by 42.44% and 17.62%, respectively. This proved that the reaction in Eq. (15) occurred and that ·OH played a major role in the oxidative degradation of HA. The addition of MeOH reduced the HA removal by 27.02% and 9.60%, respectively. This was an opposite phenomenon because MeOH could scavenge both ·OH and $SO_4^{\cdot-}$; it was a more effective radical quencher compared to TBA. This is explained by the low adsorption capacity of biochar for MeOH [6,55]. The radicals generated on the Fe-BC surface, which reduced the likelihood of MeOH contacting the radicals. Finally, the contribution of radicals was calculated at high concentration conditions [42], and the degradation of HA was dominated by the radical pathway with the contribution of ·OH (26.74%) and $SO_4^{\cdot-}$ (about 9.85%).

In addition, Fe-BC/PMS pretreatment reduced the electronegativity of HA from -30.6 mV to -26.0 mV, which enabled the electrostatic adsorption of negatively charged HA and Fe-BC, and enhanced the coagulation effect between the *in situ* generated Fe(III) (see Eq. (16)) and organic matter [10]:

$$SO_4^{\cdot-} + OH^- \rightarrow \cdot OH + SO_4^{2-} \quad (15)$$

$$Fe(II) + HSO_5^- \rightarrow Fe(III) + SO_4^{\cdot-} + OH^- \quad (16)$$

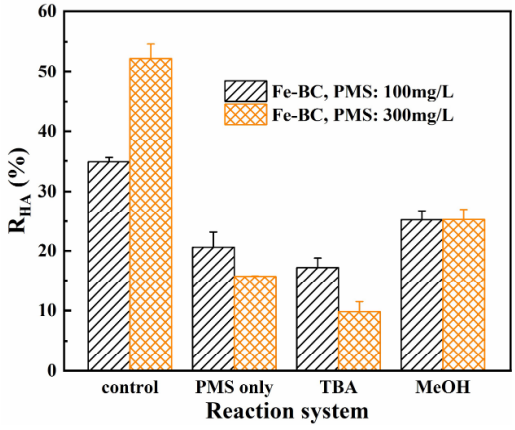

Fig. 5. Effect of MeOH and TBA on HA removal

3.2.4. Stability, reusability and regeneration of Fe-BC

The stability, reusability, and regeneration performance of Fe-BC were investigated under three agent concentration conditions. As shown in Fig. 6a, the storage time had virtually no effect on the catalytic performance of Fe-BC, which indicated that the catalysts retained good stability. The effects of new-born, reuse and regeneration catalyst on HA removal are shown in Fig. 6b. The reused catalysts diminished the HA removal rate by about 7%, possibly attributed to changes in the chemical structure of the surface, depletion of active sites, and coverage of the surface by reaction intermediates [56]. The performance of regenerated catalyst did improve to a certain extent compared with the reused catalyst. This might be attributed to the elimination of organic intermediates covering the catalyst surface. However, the desorption of iron oxides, and decomposition of oxygen-containing functional groups caused by repeated high temperatures did cause irreversible damage to Fe-BC [6]. Based on the above results, Fe-BC has good reusability and regeneration.

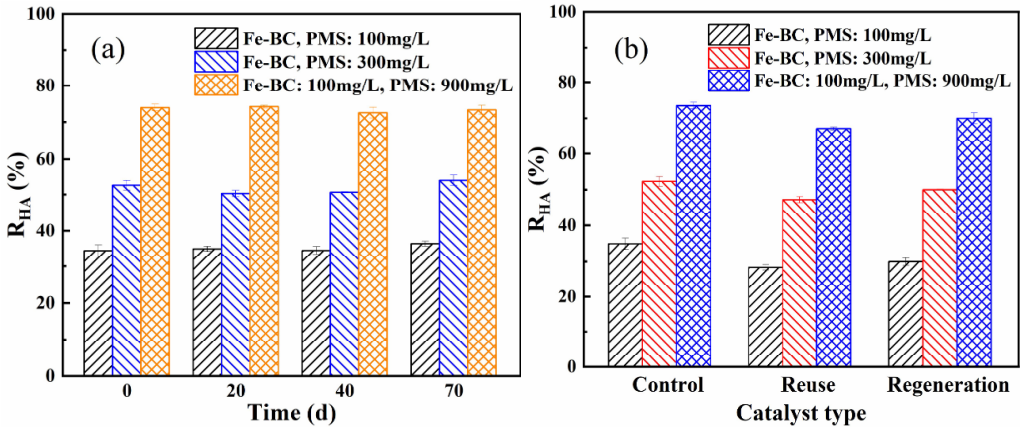

Fig. 6. Stability (a), reusability and regeneration (b) of Fe-BC.

3.3. Effects of Fe-BC/PMS pretreatment on membrane fouling

3.3.1. Trans-membrane pressure

The effectiveness of the Fe-BC/PMS/UF coupling system in mitigating membrane fouling was investigated by filtration experiments. As shown in Fig. 7a, the raw water showed a near-exponential increase in TMP curve during the filtration cycle. The TMP increased from an initial 16.3 Kpa to 52.2 Kpa within the first hour. As filtration proceeded, the TMP growth rate accelerated to a final TMP of 140.8 Kpa at the end of

filtration, which was 8.6 times the initial membrane pressure. It was noteworthy that HA solution pretreated by PMS alone and BC/PMS caused more severe membrane fouling, with final TMPs of 168.5 and 156.5 Kpa at the end of filtration, 10.6 and 9.4 times higher than the initial one, respectively. This might be due to the incomplete degradation of HA via the reaction system, where large-MW humic-like substances were partially broken down to medium-MW organic matter, leading to more serious cake layer fouling and standard blocking. However, Fe-BC/PMS pretreatment significantly alleviated the growth rate of TMP with the final TMP of 90.9 Kpa after 2 h, which was 50.0 Kpa lower compared to that of the UF system with no pretreatments.

In addition, multi-cycle filtration experiments were conducted to more realistically reflect the effectiveness of the pretreatment coupled with UF in mitigate membrane fouling. As shown in Fig. 7b, the untreated HA showed a relatively slow TMP growth of 68.1 Kpa during the first two cycles. The TMP recovered to 90% of the initial value after backwashing. However, as filtration proceeded, the TMP curve increased in a nearly linearly and reached the pressure limit of 150.0 Kpa after 4.75 h. This was due to the rapid accumulation of large-MW substances on UF membrane surface, which caused severe cake layer fouling and membrane pore blockage. For the PMS alone and BC/PMS pretreatment systems, although no mitigation appeared during the first two filtration cycles, a significant reduction in the TMP could be subsequently seen, with TMPs of 135.0 and 120.0 Kpa after 5 h, respectively. So both systems effectively mitigated the rate of membrane fouling. The Fe-BC/PMS pretreatment system had the flattest TMP curve growth and showed significantly attenuated membrane fouling in all cycles. The TMP at the end of filtration was 79.8 Kpa, reducing to about 70.0 Kpa compared to that of the UF system with no pretreatments.

3.3.2. Fouling reversibility analysis

The fouling reversibility distribution is shown in Fig. 7c. The membrane fouling resistance of raw water in each filtration cycle was almost always composed of reversible fouling. This was because the unpretreated HA contains more organic matters with molecular weight greater than 100 KDa, which was easily intercepted by membrane pores and accumulated on the membrane surface, forming a dense cake layer, resulting in serious reversible fouling rather than irreversible [10]. It reached 6.15×10^{4} m^{-1} at the end of the fourth cycle. As exhibited in Fig. 7c, the three pretreatment systems significantly reduced reversible membrane fouling after four cycles, especially Fe-BC/PMS pretreatment. Its total and reversible membrane fouling resistance was 4.08×10^{4} m^{-1} and

2.40×10^4 m^{-1}, respectively, revealing a reduction of 44% and 61%. At the same time, pretreatments slightly increased irreversible membrane fouling. Because the dense cake layer had a certain retention capacity, cake layer fouling was overcome after pretreatment, while the resulting small molecule organics entered the membrane pores causing standard blocking [57]. Despite this, Fe-BC/PMS pretreatment was an effective measure to reduce membrane resistance and prolong the filtration time of the UF membrane (see Fig. 7b).

3.3.3. Membrane fouling index analysis

Finally, the membrane fouling index (FI) was used as an indicator to visually represent the degree of membrane fouling during cyclic filtration (see Fig. 7d). Clearly, the FI of raw water generally tended to increase over the five filtration cycles, meaning that its membrane fouling rate got faster as time passed. The FI of the three pretreatment systems all displayed different decreasing trends, and the Fe-BC/PMS pretreatment system mitigated membrane fouling the best.

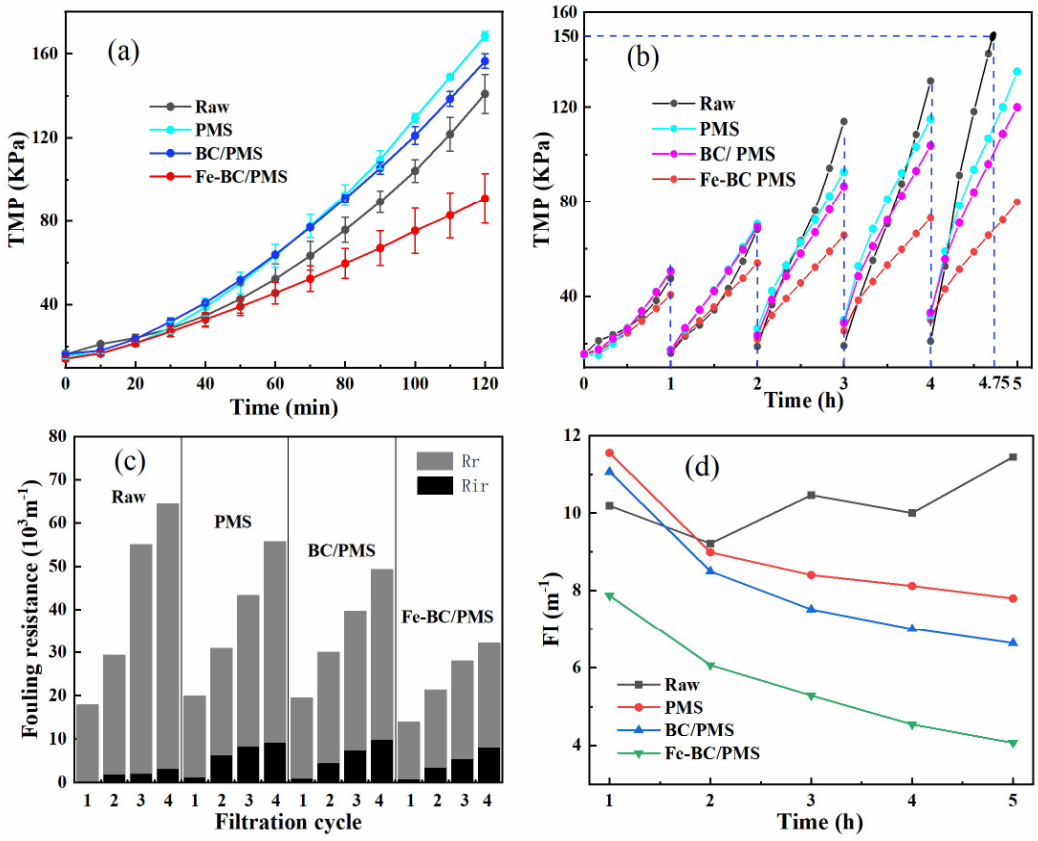

Fig. 7. Effects of pretreatment on membrane fouling: single cycle (a) and multi-cycle TMP curves (b), fouling resistance distribution (c), and FI curves (d).

3.4. Membrane fouling mitigation pathways

Pretreatment can mitigate membrane fouling in many ways. Firstly, after three different pretreatment methods, the SUVA of HA dropped to varying degrees (see Fig. S6a). This meant that the pretreatment preferentially removed organic matter containing unsaturated bonds and aromatic rings. The hydrophobic component of HA molecule was transformed into a more hydrophilic organic matter, which reduced the adhesion of HA to the UF membrane [58]. Therefore, pretreatment-induced changes in the structure and properties of HA helped to ameliorate cake layer fouling and standard blocking of the UF membrane.

Secondly, the effect of HA removal rate on membrane fouling during Fe-BC/PMS pretreatment is shown in Fig. S6b. As the reaction proceeded, the HA concentration gradually decreased (see Fig. 4b), and the TMP also showed a decreasing trend at the end of the single-cycle filtration experiment. In particular, after 1, 2, and 8 h of reaction, the TMP significantly reduced, which indicated membrane fouling was effectively alleviated. To analyze the relationship between the HA removal rate and the extent of membrane fouling, the DOC and λ of HA solutions over reaction time were measured and fitted to the FI, respectively (see Fig. S6c). The R^2 of FI with DOC and λ were 0.87 and 0.38, respectively, and the membrane fouling had a high correlation with the degree of organic matter mineralization. Therefore, the mitigation of membrane fouling by Fe-BC/PMS pretreatment may be attributed to the complete degradation of some HA.

Finally, in order to better evaluate the membrane fouling process and types of fouling, five combined fouling models were devised to fit the TMP curves in HA filtration in this study. As shown in Fig. 8, except for the complete-standard blocking model with a minimal degree of fit, all the other models fitted by HA raw water had a high correlation. Of these the cake-intermediate and intermediate-standard blocking model had the best fit with correlation coefficients R^2 greater than 0.999. This indicated that the membrane fouling was caused by a combination of multiple fouling forms (mainly intermediate blocking). After pretreatment, the correlation of the TMP curve with the complete-standard blocking model decreased, while it still remained strong with the other four models (R^2 >0.98). The complete blocking parameter (K_b) and standard blocking parameter (Ks) of the complete-standard blocking model are shown in Table S3. The K_b/Ks values had fallen to different degrees after pretreatment, indicating that a shift had occurred from complete to standard blocking. This might be the key to dealing with membrane fouling mitigation. These results further strongly suggested that larger organic substances were broken down into smaller MW organics or mineralized. Therefore, this

directly alleviated complete blocking while some low-MW organics entered membrane pores which caused standard blocking.

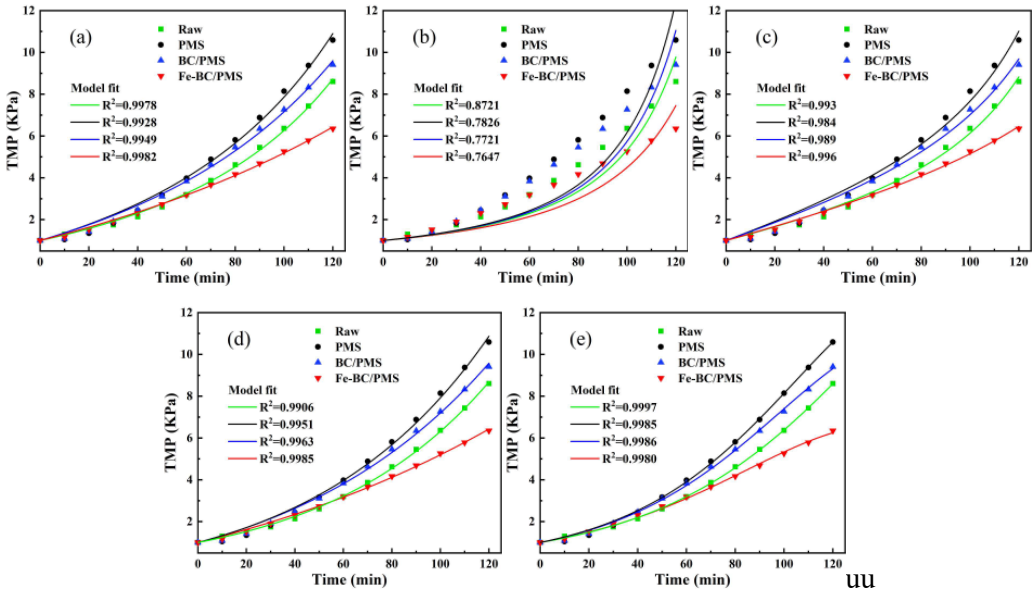

uu

Fig. 8. Membrane fouling model fitting: cake-complete model (a); complete-standard model (b); cake-standard model (c); cake-intermediate model (d); intermediate-standard model (e).

4. Conclusions

Fe-BC was prepared by co-precipitation for activating PMS as pretreatment before UF. As a catalyst in the pH range of 5~9, it could effectively activate PMS to degrade HA in a short time. Radical quenching experiments revealed that $SO_4^{\cdot-}$ and ·OH were jointly involved in the degradation of HA. Its stability, reusability and regeneration highlighted good prospects for the Fe-BC /PMS pretreatment. Five cycle filtration experiments revealed that Fe-BC /PMS pretreatment effectively mitigated TMP growth rates and significantly reduced total (44%) and reversible (61%) fouling of UF membrane. The longer reaction time helped mitigate membrane fouling while the combined membrane fouling model fit indicated that pretreatment shifted the complete blocking to standard blocking. Therefore, the mitigation of membrane fouling caused by HA may be attributed to the alleviation of complete fouling. In short, the Fe-BC/PMS/UF combined process performed well in removing HA and dealing with membrane fouling. Its prospects for water purification are very encouraging.

Acknowledgements

This research was supported by Tianjin Municipal Science and Technology Bureau of China (grant numbers 20JCZDJC00380 and 18PTZWHZ00140).

References:

[1] N. Lee, G. Amy, J.-P. Croué, H. Buisson, Identification and understanding of fouling in low-pressure membrane (MF/UF) filtration by natural organic matter (NOM), Water Res. 38 (2004) 4511-4523, https://doi.org/10.1016/j.watres.2004.08.013.

[2] D. Jermann, W. Pronk, S. Meylan, M. Boller, Interplay of different NOM fouling mechanisms during ultrafiltration for drinking water production, Water Res. 41 (2007) 1713-1722, https://doi.org/10.1016/j.watres.2006.12.030.

[3] G. Amy, Fundamental understanding of organic matter fouling of membranes, Desalination 231 (2008) 44-51, https://doi.org/10.1016/j.desal.2007.11.037.

[4] K. Li, H. Liang, F. Qu, S. Shao, H. Yu, Z.-s. Han, X. Du, G. Li, Control of natural organic matter fouling of ultrafiltration membrane by adsorption pretreatment: Comparison of mesoporous adsorbent resin and powdered activated carbon, J. Membr. Sci. 471 (2014) 94-102, https://doi.org/10.1016/j.memsci.2014.08.006.

[5] T. Moriguchi, K. Yano, M. Tahara, K. Yaguchi, Metal-modified silica adsorbents for removal of humic substances in water, J. Colloid Interface Sci. 283 (2005) 300-310, https://doi.org/10.1016/j.jcis.2004.09.019.

[6] L. Chen, X. Ren, Y. Li, D. Hu, X. Feng, Y. Liu, J. Zhao, High flux Fe/activated carbon membranes for efficient degradation of organic pollutants in water by activating sodium persulfate, Sep. Purif. Technol. 285 (2022), 120411, https://doi.org/10.1016/j.seppur.2021.120411.

[7] X.-F. Li, W.A. Mitch, Drinking Water Disinfection Byproducts (DBPs) and Human Health Effects: Multidisciplinary Challenges and Opportunities, Environ. Sci. Technol. 52 (2018) 1681-1689, https://doi.org/10.1021/acs.est.7b05440.

[8] S.E. Hrudey, L.C. Backer, A.R. Humpage, S.W. Krasner, D.S. Michaud, L.E. Moore, P.C. Singer, B.D. Stanford, Evaluating Evidence for Association of Human Bladder Cancer with Drinking-Water Chlorination Disinfection By-Products, Journal of Toxicology and Environmental Health, Part B 18 (2015) 213-241, https://doi.org/10.1080/10937404.2015.1067661.

[9] Q. Li, M. Elimelech, Synergistic effects in combined fouling of a loose nanofiltration membrane by colloidal materials and natural organic matter, J. Membr. Sci. 278 (2006) 72-82, https://doi.org/10.1016/j.memsci.2005.10.045.

[10] W. Gao, H. Liang, J. Ma, M. Han, Z.-l. Chen, Z.-s. Han, G.-b. Li, Membrane fouling control in ultrafiltration technology for drinking water production: A review, Desalination 272 (2011) 1-8, https://doi.org/10.1016/j.desal.2011.01.051.

[11] C. Yu, B. Gao, W. Wang, X. Xu, Q. Yue, Alleviating membrane fouling of modified polysulfone membrane via coagulation pretreatment/ultrafiltration hybrid process, Chemosphere 235 (2019) 58-69, https://doi.org/10.1016/j.chemosphere.2019.06.146.

[12] B. Malczewska, M.M. Benjamin, Efficacy of hybrid adsorption/membrane pretreatment for low pressure membrane, Water Res. 99 (2016) 263-271, https://doi.org/10.1016/j.watres.2016.04.065.

[13] P. Jutaporn, P.C. Singer, R.M. Cory, O. Coronell, Minimization of short-term low-pressure membrane fouling using a magnetic ion exchange (MIEX®) resin, Water Res. 98 (2016) 225-234, https://doi.org/10.1016/j.watres.2016.04.007.

[14] J. Xing, L. Du, X. Quan, X. Luo, S.A. Snyder, H. Liang, Combining chlor(am)ine-UV oxidation to ultrafiltration for potable water reuse: Promoted efficiency, membrane fouling control and mechanism, J. Membr. Sci. 635 (2021), 119511, https://doi.org/10.1016/j.memsci.2021.119511.

[15] Y. Wan, P. Xie, Z. Wang, J. Wang, J. Ding, R. Dewil, B. Van der Bruggen, Application of UV/chlorine pretreatment for controlling ultrafiltration (UF) membrane fouling caused by different natural organic fractions, Chemosphere 263 (2021), 127993, https://doi.org/10.1016/j.chemosphere.2020.127993.

[16] B. Ma, X. Wang, R. Liu, W.A. Jefferson, H. Lan, H. Liu, J. Qu, Synergistic process using Fe hydrolytic flocs and ultrafiltration membrane for enhanced antimony(V) removal, J. Membr. Sci. 537 (2017) 93-100, https://doi.org/10.1016/j.memsci.2017.05.022.

[17] A. Imbrogno, A. Tiraferri, S. Abbenante, S. Weyand, R. Schwaiger, T. Luxbacher, A.I. Schäfer, Organic fouling control through magnetic ion exchange-nanofiltration (MIEX-NF) in water treatment, J. Membr.

Sci. 549 (2018) 474-485, https://doi.org/10.1016/j.memsci.2017.12.041.
[18] S. Mikhaylin, L. Bazinet, Fouling on ion-exchange membranes: Classification, characterization and strategies of prevention and control, Adv. Colloid Interface Sci. 229 (2016) 34-56, https://doi.org/10.1016/j.cis.2015.12.006.
[19] X. Cheng, H. Liang, A. Ding, F. Qu, S. Shao, B. Liu, H. Wang, D. Wu, G. Li, Effects of pre-ozonation on the ultrafiltration of different natural organic matter (NOM) fractions: Membrane fouling mitigation, prediction and mechanism, J. Membr. Sci. 505 (2016) 15-25, https://doi.org/10.1016/j.memsci.2016.01.022.
[20] S. Ziembowicz, M. Kida, Limitations and future directions of application of the Fenton-like process in micropollutants degradation in water and wastewater treatment: A critical review, Chemosphere (2022) 134041, https://doi.org/10.1016/j.chemosphere.2022.134041.
[21] R. Miao, Y. Feng, Y. Wang, P. Wang, P. Li, X. Li, L. Wang, Exploring the influence mechanism of ozonation on protein fouling of ultrafiltration membranes as a result of the interfacial interaction of foulants at the membrane surface, Sci. Total Environ. 785 (2021), 147340, https://doi.org/10.1016/j.scitotenv.2021.147340.
[22] D. Hou, D. Lin, C. Zhao, J. Wang, C. Fu, Control of protein (BSA) fouling by ultrasonic irradiation during membrane distillation process, Sep. Purif. Technol. 175 (2017) 287-297, https://doi.org/10.1016/j.seppur.2016.11.047.
[23] H. Zhang, J. Zhang, J. Luo, Y. Wan, A novel paradigm of photocatalytic cleaning for membrane fouling removal, J. Membr. Sci. 641 (2022) 119859, https://doi.org/10.1016/j.memsci.2021.119859.
[24] B.A. Nerger, R.H. Peiris, C. Moresoli, Fluorescence analysis of NOM degradation by photocatalytic oxidation and its potential to mitigate membrane fouling in drinking water treatment, Chemosphere 136 (2015) 140-144, https://doi.org/10.1016/j.chemosphere.2015.03.089.
[25] U. Ushani, X. Lu, J. Wang, Z. Zhang, J. Dai, Y. Tan, S. Wang, W. Li, C. Niu, T. Cai, N. Wang, G. Zhen, Sulfate radicals-based advanced oxidation technology in various environmental remediation: A state-of-the–art review, Chem. Eng. J. 402 (2020), 126232, https://doi.org/10.1016/j.cej.2020.126232.
[26] H. Liu, M. Ye, X. Dong, Z. Ren, S. Long, E. Lichtfouse, Removal of humic substances by the synergistic effect of biochar adsorption and activation of persulfate, J. Water Process Eng. 44 (2021), 102428, https://doi.org/10.1016/j.jwpe.2021.102428.
[27] Y. Zhao, X. Yuan, X. Li, L. Jiang, H. Wang, Burgeoning prospects of biochar and its composite in persulfate-advanced oxidation process, J. Hazard. Mater. 409 (2021), 124893, https://doi.org/10.1016/j.jhazmat.2020.124893.
[28] X. Li, C. Wang, J. Zhang, J. Liu, B. Liu, G. Chen, Preparation and application of magnetic biochar in water treatment: A critical review, Sci. Total Environ. 711 (2020), 134847, https://doi.org/10.1016/j.scitotenv.2019.134847.
[29] H. Huang, T. Guo, K. Wang, Y. Li, G. Zhang, Efficient activation of persulfate by a magnetic recyclable rape straw biochar catalyst for the degradation of tetracycline hydrochloride in water, Sci. Total Environ. 758 (2021), 143957, https://doi.org/10.1016/j.scitotenv.2020.143957.
[30] J. Ye, Y. Wang, Z. Li, D. Yang, C. Li, Y. Yan, J. Dai, 2D confinement freestanding graphene oxide composite membranes with enriched oxygen vacancies for enhanced organic contaminants removal via peroxymonosulfate activation, J. Hazard. Mater. 417 (2021), 126028, https://doi.org/10.1016/j.jhazmat.2021.126028.
[31] C.-F. Lin, A. Yu-Chen Lin, P. Sri Chandana, C.-Y. Tsai, Effects of mass retention of dissolved organic matter and membrane pore size on membrane fouling and flux decline, Water Res. 43 (2009) 389-394, https://doi.org/10.1016/j.watres.2008.10.042.
[32] S.-J. Lee, M. Dilaver, P.-K. Park, J.-H. Kim, Comparative analysis of fouling characteristics of ceramic and polymeric microfiltration membranes using filtration models, J. Membr. Sci. 432 (2013) 97-105, https://doi.org/10.1016/j.memsci.2013.01.013.
[33] S. Shao, H. Liang, F. Qu, H. Yu, K. Li, G. Li, Fluorescent natural organic matter fractions responsible for ultrafiltration membrane fouling: Identification by adsorption pretreatment coupled with parallel factor analysis of excitation–emission matrices, J. Membr. Sci. 464 (2014) 33-42, https://doi.org/10.1016/j.memsci.2014.03.071.

[34] G. Bolton, D. LaCasse, R. Kuriyel, Combined models of membrane fouling: Development and application to microfiltration and ultrafiltration of biological fluids, J. Membr. Sci. 277 (2006) 75-84, https://doi.org/10.1016/j.memsci.2004.12.053.
[35] M. Yan, X. Shen, B. Gao, K. Guo, Q. Yue, Coagulation-ultrafiltration integrated process for membrane fouling control: Influence of Al species and SUVA values of water, Sci. Total Environ. 793 (2021), 148517, https://doi.org/10.1016/j.scitotenv.2021.148517.
[36] X. Zhang, Y. Zhang, H.H. Ngo, W. Guo, H. Wen, D. Zhang, C. Li, L. Qi, Characterization and sulfonamide antibiotics adsorption capacity of spent coffee grounds based biochar and hydrochar, Sci. Total Environ. 716 (2020), 137015, https://doi.org/10.1016/j.scitotenv.2020.137015.
[37] R. Gurav, S.K. Bhatia, T.-R. Choi, Y.-L. Park, J.Y. Park, Y.-H. Han, G. Vyavahare, J. Jadhav, H.-S. Song, P. Yang, J.-J. Yoon, A. Bhatnagar, Y.-K. Choi, Y.-H. Yang, Treatment of furazolidone contaminated water using banana pseudostem biochar engineered with facile synthesized magnetic nanocomposites, Bioresour. Technol. 297 (2020), 122472, https://doi.org/10.1016/j.biortech.2019.122472.
[38] Y. Zhou, S. Cao, C. Xi, X. Li, L. Zhang, G. Wang, Z. Chen, A novel Fe_3O_4/graphene oxide/citrus peel-derived bio-char based nanocomposite with enhanced adsorption affinity and sensitivity of ciprofloxacin and sparfloxacin, Bioresour. Technol. 292 (2019), 121951, https://doi.org/10.1016/j.biortech.2019.121951.
[39] X. Pan, Z. Gu, W. Chen, Q. Li, Preparation of biochar and biochar composites and their application in a Fenton-like process for wastewater decontamination: A review, Sci. Total Environ. 754 (2021), 142104, https://doi.org/10.1016/j.scitotenv.2020.142104.
[40] J. Du, J. Bao, Y. Liu, S.H. Kim, D.D. Dionysiou, Facile preparation of porous Mn/Fe3O4 cubes as peroxymonosulfate activating catalyst for effective bisphenol A degradation, Chem. Eng. J. 376 (2019), 119193, https://doi.org/10.1016/j.cej.2018.05.177.
[41] B. Wang, Y.-n. Li, L. Wang, Metal-free activation of persulfates by corn stalk biochar for the degradation of antibiotic norfloxacin: Activation factors and degradation mechanism, Chemosphere 237 (2019), 124454, https://doi.org/10.1016/j.chemosphere.2019.124454.
[42] X. Zhang, Y. Yang, H. Hao Ngo, W. Guo, T. Long, X. Wang, J. Zhang, F. Sun, Enhancement of urea removal from reclaimed water using thermally modified spent coffee ground biochar activated by adding peroxymonosulfate for ultrapure water production, Bioresour. Technol. 349 (2022), 126850, https://doi.org/10.1016/j.biortech.2022.126850.
[43] Z. Han, J. Huo, X. Zhang, H.H. Ngo, W. Guo, Q. Du, Y. Zhang, C. Li, D. Zhang, Characterization and flocculation performance of a newly green flocculant derived from natural bagasse cellulose, Chemosphere 301 (2022), 134615, https://doi.org/10.1016/j.chemosphere.2022.134615.
[44] C. Liang, H.-W. Su, Identification of Sulfate and Hydroxyl Radicals in Thermally Activated Persulfate, Industrial & Engineering Chemistry Research 48 (2009) 5558-5562, https://doi.org/10.1021/ie9002848.
[45] S. Yang, P. Wang, X. Yang, L. Shan, W. Zhang, X. Shao, R. Niu, Degradation efficiencies of azo dye Acid Orange 7 by the interaction of heat, UV and anions with common oxidants: Persulfate, peroxymonosulfate and hydrogen peroxide, J. Hazard. Mater. 179 (2010) 552-558, https://doi.org/10.1016/j.jhazmat.2010.03.039.
[46] N. Liu, F. Ding, C.-H. Weng, C.-C. Hwang, Y.-T. Lin, Effective degradation of primary color direct azo dyes using Fe0 aggregates-activated persulfate process, J. Environ. Manage. 206 (2018) 565-576, https://doi.org/10.1016/j.jenvman.2017.11.006.
[47] S. Yang, P. Wu, J. Liu, M. Chen, Z. Ahmed, N. Zhu, Efficient removal of bisphenol A by superoxide radical and singlet oxygen generated from peroxymonosulfate activated with Fe0-montmorillonite, Chem. Eng. J. 350 (2018) 484-495, https://doi.org/10.1016/j.cej.2018.04.175.
[48] S. Popova, G. Matafonova, V. Batoev, Simultaneous atrazine degradation and E. coli inactivation by UV/$S_2O_8^{2-}$/Fe^{2+} process under KrCl excilamp (222 nm) irradiation, Ecotoxicology and Environmental Safety 169 (2019) 169-177, https://doi.org/10.1016/j.ecoenv.2018.11.014.
[49] Y.F. Rao, L. Qu, H. Yang, W. Chu, Degradation of carbamazepine by Fe(II)-activated persulfate process, J. Hazard. Mater. 268 (2014) 23-32, https://doi.org/10.1016/j.jhazmat.2014.01.010.
[50] A. Li, Z. Wu, T. Wang, S. Hou, B. Huang, X. Kong, X. Li, Y. Guan, R. Qiu, J. Fang, Kinetics and mechanisms of the degradation of PPCPs by zero-valent iron (Fe^0) activated peroxydisulfate (PDS) system

in groundwater, J. Hazard. Mater. 357 (2018) 207-216, https://doi.org/10.1016/j.jhazmat.2018.06.008.
[51] S. Xiao, M. Cheng, H. Zhong, Z. Liu, Y. Liu, X. Yang, Q. Liang, Iron-mediated activation of persulfate and peroxymonosulfate in both homogeneous and heterogeneous ways: A review, Chem. Eng. J. 384 (2020), 123265, https://doi.org/10.1016/j.cej.2019.123265.
[52] H. Dong, K. Hou, W. Qiao, Y. Cheng, L. Zhang, B. Wang, L. Li, Y. Wang, Q. Ning, G. Zeng, Insights into enhanced removal of TCE utilizing sulfide-modified nanoscale zero-valent iron activated persulfate, Chem. Eng. J. 359 (2019) 1046-1055, https://doi.org/10.1016/j.cej.2018.11.080.
[53] Z. Li, S. Luo, Y. Yang, J. Chen, Highly efficient degradation of trichloroethylene in groundwater based on peroxymonosulfate activation by bentonite supported Fe/Ni bimetallic nanoparticle, Chemosphere 216 (2019) 499-506, https://doi.org/10.1016/j.chemosphere.2018.10.133.
[54] Y. Zhang, Q. Jiang, S. Jiang, H. Li, R. Zhang, J. Qu, S. Zhang, W. Han, One-step synthesis of biochar supported nZVI composites for highly efficient activating persulfate to oxidatively degrade atrazine, Chem. Eng. J. 420 (2021), 129868, https://doi.org/10.1016/j.cej.2021.129868.
[55] R. Matta, H. Younes, R. Hanna, J. Saab, R. Abou-Khalil, Sulfate radicals mediated oxidation of amoxicillin: Optimization of key parameters, J. Environ. Manage. 245 (2019) 375-383, https://doi.org/10.1016/j.jenvman.2019.05.030.
[56] X. Rong, M. Xie, L. Kong, V. Natarajan, L. Ma, J. Zhan, The magnetic biochar derived from banana peels as a persulfate activator for organic contaminants degradation, Chem. Eng. J. 372 (2019) 294-303, https://doi.org/10.1016/j.cej.2019.04.135.
[57] K. Kimura, K. Kume, Irreversible fouling in hollow-fiber PVDF MF/UF membranes filtering surface water: Effects of precoagulation and identification of the foulant, J. Membr. Sci. 602 (2020), 117975, https://doi.org/10.1016/j.memsci.2020.117975.
[58] S. Van Geluwe, L. Braeken, B. Van der Bruggen, Ozone oxidation for the alleviation of membrane fouling by natural organic matter: A review, Water Res. 45 (2011) 3551-3570, https://doi.org/10.1016/j.watres.2011.04.016.